JMEPEG (2006) 15:661-667
DOI: 10.1361/105994906X150759

1059-9495/$19.00

Evaluating the Berkovitz Method to Predict Fatigue Loads in Mechanical Failure Investigations

C.O.F.T. Ruckert, J.R. Tarpani, M.T. Milan, W.W. Bose Filho, and D. Spinelli

(Submitted November 30, 2005; in revised form January 20, 2006)

This article evaluates a proposed analytical-experimental methodology by which the fatigue load levels leading to failure of structural components is inferred. The so-called Berkovitz method is recognized to depend fundamentally on a 1:1 relationship of micro- and macroscopic crack propagation rates. Compact tensile specimens of a high-strength aluminum alloy were fatigue tested at room temperature according to ASTM-E647, in plane-stress and plane-strain conditions, respectively. Unloading elastic compliance and low-magnification visual techniques monitored crack propagation rates. Topographical survey of fractured surfaces was carried out in a scanning electron microscope to measure striation spacing at constant-ΔK locations. By inputting these values in the Berkovitz model, the load spectrum applied during the fatigue testing could be derived. Research results have shown that, if correctly and carefully used, the assessed procedure provides accurate estimation of fatigue loads, so constituting a powerful tool during failure analysis of mechanical components operating in constant amplitude loading conditions.

Keywords accident failure investigation, Berkovitz's method, fatigue crack growth, fatigue striation spacing, quantitative fractography

1. Introduction

Structural fatigue failures are responsible for most of the accidents involving fracture. Despite the efforts used by Kitagawa and Koterazawa (Ref 1, 2) in estimating in-service loads by striation spacing analysis of the fractured surfaces by scanning electron microscopy (SEM) techniques (Fig. 1), it is now well recognized that the load levels leading to subcritical crack growth can not be deduced by postmortem inspection of the fractured surface only.

More recently, Berkovitz (Ref 3) has proposed an analytical-experimental method, hereafter named "K-parameterization method," to infer fatigue loads in failure investigations. In this methodology, summarized in Fig. 2, da/dN versus ΔK curves are determined for the material by conventional fatigue testing in the laboratory environment. Alternatively, this information can be assessed in technical databanks, which describe most of the engineering metals and alloys. Still in Fig. 2, the K-solution is supplied for a superficial crack in the structural component of interest, which is known to be fatigue loaded in testing or in-service conditions. Analytical and numerical methods are frequently used in deriving these stress intensity solutions, which are well documented in the literature for the most common structural configurations. K-parameterization, regarding both the small-scale test specimen and the full-size cracked body, allows one to plot load or stress as a function of the crack length, a. If the striation spacing, S (i.e., the microscopic crack growth rate determined [at a known location, say a*, from the crack site] over the fractured surface from the

C.O.F.T. Ruckert, J.R. Tarpani, M.T. Milan, W.W. Bose Filho, and **D. Spinelli,** Materials, Aeronautics and Automotive Engineering Department, Engineering School of São Carlos, University of São Paulo, Brazil. Contact e-mail: cassius@sc.usp.br.

Symbols and Nomenclature

a	crack length or depth
AMS	Aerospace Material Specification
ASTM	American Society for Testing and Materials
A_0	original gage cross-sectional area
C(T)	compact tensile specimen
C	Paris coefficient
Cs	Miller coefficient
C'	Ritchie and Rao coefficient
E	Young's modulus
EL_F	elongation at fracture
f	frequency of application of fatigue loading cycles
G	general or global crack growth direction
K	stress intensity factor
K_{IC}	fracture toughness
L	local crack growth direction
Lt	load orientation (see orientation in ASTM 399-00)
L_0	original gage length
MTS	Materials Testing System
m	Paris exponent – slope of the Paris curve
m_s	Miller exponent – slope of the Miller curve
m_r	Ritchie and Rao exponent – slope of the Ritchie and Rao curve
R	fatigue load ratio
RA_F	reduction in area at fracture
S	fatigue striation spacing
S_G	fatigue striation spacing in G (global or general) direction
S_L	fatigue striation spacing in L (local) direction
SAE	Society of Automotive Engineers
SEM	scanning electron microscope
S_U	ultimate tensile strength
S_Y	0.2% offset yield strength
T	compact specimen's thickness
ΔK	range of stress intensity factor
ΔK_{th}	threshold range of stress intensity factor
ΔP	range of mechanical load
ϕ	displacement angle between G and L directions
σ	nominal tensile stress

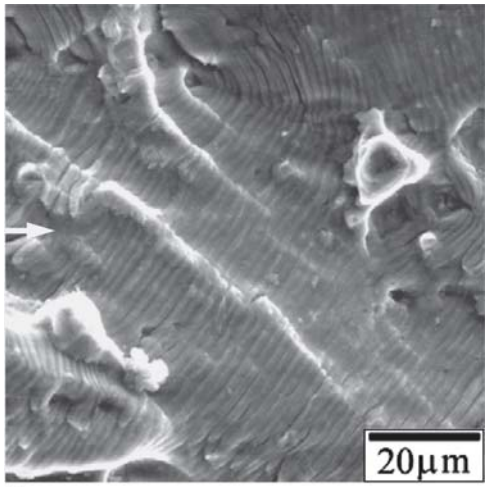

(a)

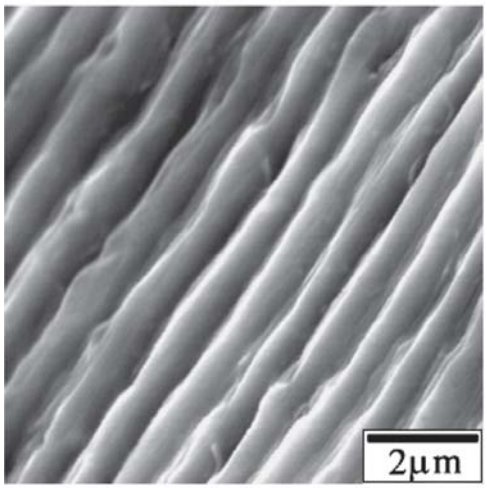

(b)

Fig. 1 (a) Low and (b) high magnification images of typical fatigue striation patterns developed in high-strength Al-alloys subjected to constant-stress amplitude loading. Arrows indicate the macroscopic crack growth directions.

topographical survey of a structural component failed by fatigue mechanism), can be correlated to the macroscopic crack growth speed, d*a*/d*N*, the load or stress levels that occurred during the fatigue fracture of the structural component is promptly available.

In this work, fatigue tests under constant amplitude loading have been performed using C(T) compact specimens in both plane-stress and plane-strain conditions, for a 7475-T7351 aluminum alloy. The fractured surfaces were carefully inspected in a SEM, to verify the validity of the Berkovitz procedure, which is dependent on the 1:1 relationship between the microscopic, *S*, and macroscopic, d*a*/d*N*, crack growth rates.

According to Broek (Ref 4), and more recently to Nedbal (Ref 5), such correlation is valid within the fatigue crack growth rate range from 0.1 to 1 μm per cycle only. Above this range, d*a*/d*N* is increased by the monotonic component of failure due to microvoid nucleation and/or local cleavage triggered in the vicinity of intermetallic particles. Below this range, *S* is larger than d*a*/d*N* due to the irregularities of the crack front and/or idle load cycles, which do not result in effective crack growth.

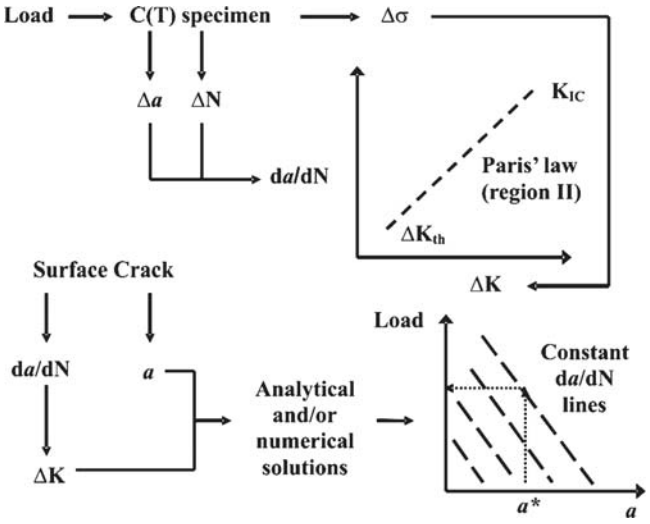

Fig. 2 K-parameterization method, based on the K-singularity of linear elastic stress-strain fields originated at the crack tip, in C(T) specimens or structural parts (Ref 3)

Table 1 Chemical composition of the 7475-T7351 aluminum alloy (wt%)

Si	Fe	Cu	Mn	Mg	Cr	Ni	Zn	P	Al
0.047	0.065	1.763	0.003	1.949	0.239	0.005	5.793	0.010	bal

Table 2 Tensile properties of the 7475-T7351 aluminum alloy tested at room temperature

	E, GPa	S_U, MPa	S_Y, MPa	RA_F(a), %	EL_F(b), %
Average of 4 tests	71.4	469.8	395.1	19.4	13.9
Standard deviation	7.7	13.3	13.0	3.0	0.7

(a) $A_0 = 28.8$ mm^2, (b) $L_0 = 25.0$ mm

2. Material

The material of this study consisted of a high-strength 7475 Al-alloy heat-treated for T7351 condition. The final microstructure presented an HV_{10kgf} hardness of 158 and plane-strain fracture toughness value, $K_{IC,}$ of 50MPa$\sqrt{m}$ in LT orientation, at ambient temperature (Ref 6). This alloy is extensively used in the aeronautic industry and exhibits a pronounced ductility that provides unequivocal striation patterns on the fracture surface during fatigue crack propagation.

The chemical composition of the material tested is supplied in Table 1. The alloy satisfies the specification SAE-AMS 4202C (Ref 7) for 7475-T7351 Al-alloy.

Table 2 lists the results of tensile tests performed in round specimens machined in the longitudinal orientation, in accordance with ASTM-E8M (Ref 8).

3. Experimental and Analytical

The macroscopic crack growth rate d*a*/d*N* versus Δ*K* curves were obtained by fatigue testing C(T) specimens containing a

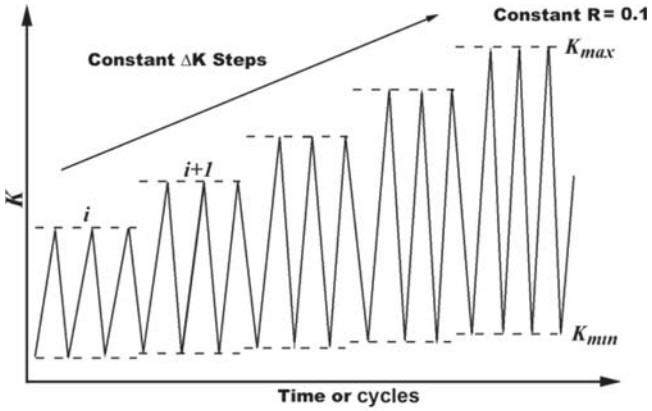

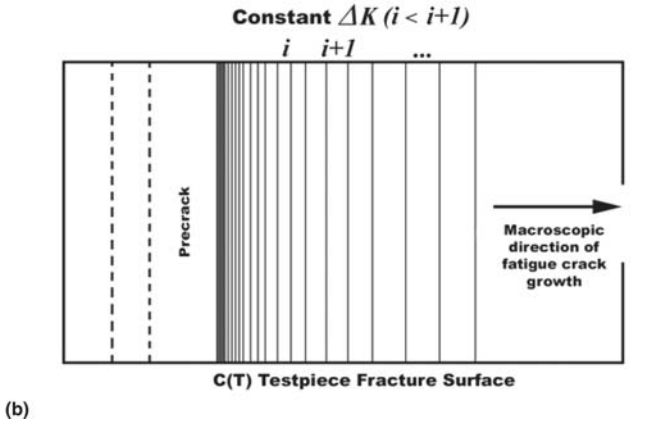

Fig. 3 (a) Applied loading spectrum in terms of K-stress intensity factor; (b) resultant striation patterns on the specimen fractured surface

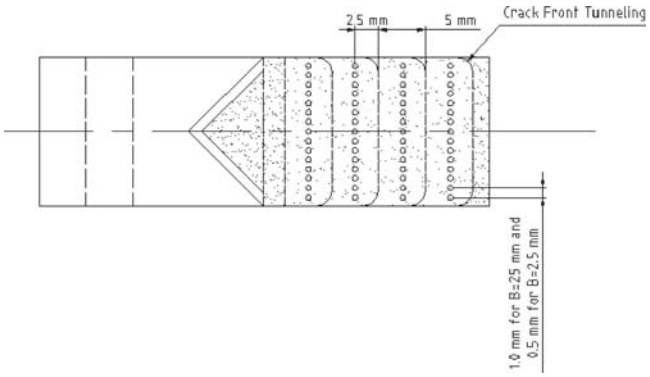

Fig. 4 Methodology for striation space imaging and measurement over the fractured surfaces of C(T) specimens for plane strain condition

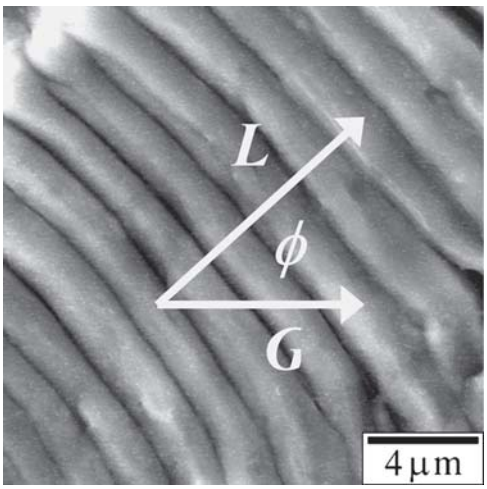

Fig. 5 Local, *L*, and general, *G*, crack growth directions

Chevron notch to induce in-plane crack propagation. To guarantee predominant plane-stress and plane-strain conditions, respectively, 2.5 mm thick (0.1T) and 25 mm thick (1T) specimens were tested. The specimens were machined in LT orientation and tested at ambient temperature, under a constant load range, ΔP (i.e., increasing ΔK tests), according to ASTM-E647 (Ref 9).

Besides the increasing ΔK tests, additional fatigue tests were performed in similar specimens in which five distinct and constant ΔK levels were applied in a stepwise manner, to allow further reading of striation spacing at constant-ΔK locations, as schematically depicted in Fig. 3. All tests were carried out under a sinusoidal waveform with a load ratio (R) of 0.1 and a frequency (f) of 20 Hz, in a servo-hydraulic closed-loop MTS 810 testing machine.

Macroscopic fatigue crack growth rates, da/dN, were determined by the unloading elastic compliance technique and by visual observation using a low-power traveler optical microscope.

For microscopic fatigue crack growth rate measurements, S, fractographic analyses of the broken specimens were performed in a SEM operating in the secondary electron imaging mode at accelerating voltage of 20 kV, without tilting the specimens (incident electron beam normal to the fracture plane). The strategy adopted for striation spacing measurements is depicted in Fig. 4 for the specimens in both plane-stress and plane-strain conditions. Conventional digital image analyzer software was used to perform a number of striation spacing measurements in the local or microscopic crack growth direction, S_L. However, only the average values of S_L and S_G along the specimen thickness have been used for deals of comparison with the macroscopic rate da/dN. According to Fig. 5, the average striation space along the general crack growth direction, S_G, is defined by:

$$S_G = S_L * \cos \phi \quad \text{(Eq 1)}$$

where ϕ is the angle between the two directions referred to previously. Observe that $S_L \geq S_G$ because S_G is the projection of S_L on the macroscopic crack growth direction, along the crack propagation curve.

The numerical or analytical procedures depicted in Fig. 2 were strictly followed in generating the K-parameterization diagram for the material and fatigue specimen tested (Ref 3).

It must be emphasized that the Berkovitz model has purposely been put at proof in this study by having as the baseline the fatigue test specimen results because strict control has been exerted in carrying out the mechanical tests as well as in determining both the respective macroscopic (da/dN) and microscopic (S_L and S_G) crack growth rates. Therefore, K-estimations in terms of the determined load range, ΔP, could be straightforwardly compared with the values actually displayed

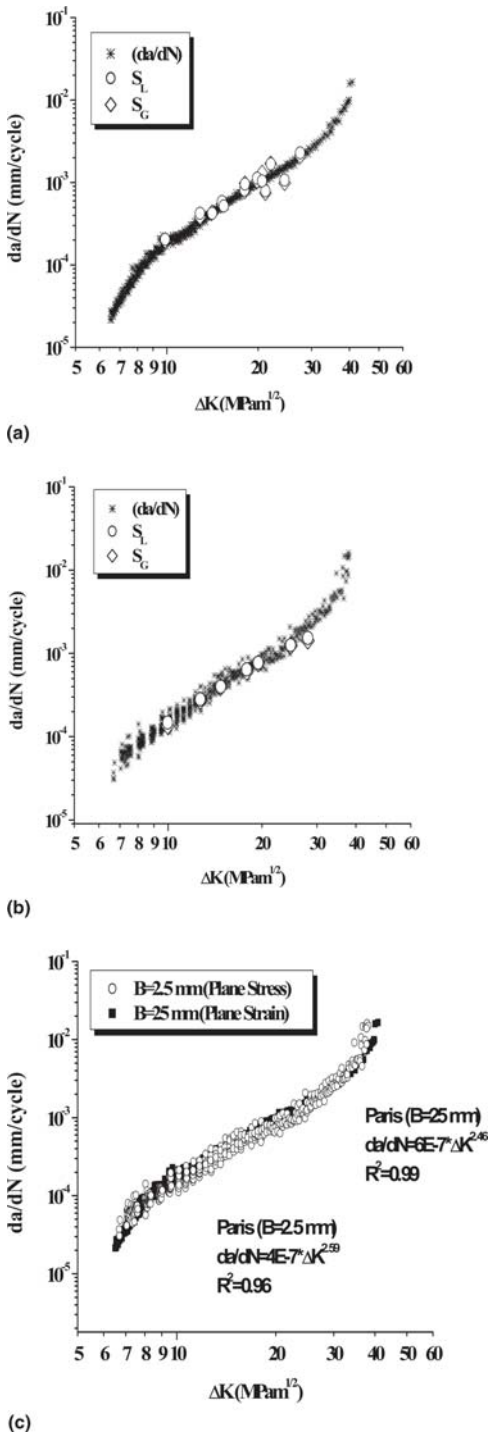

Fig. 6 Macroscopic and microscopic crack growth data for the material tested: (a) plane-strain condition; (b) plane-stress condition; (c) macrocrack growth results for both conditions, plane strain and plane stress

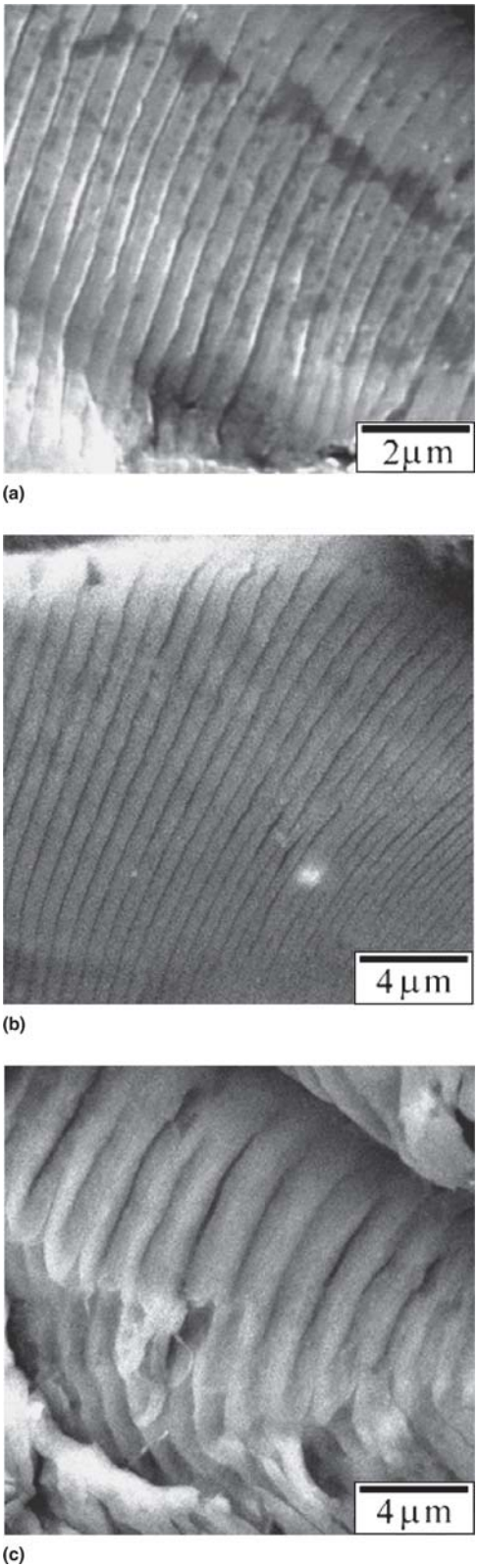

Fig. 7 Fatigue striation formed at constant ΔK levels: (a) 18 MPa$\sqrt{m}$; (b) 20 MPa$\sqrt{m}$; and (c) 22 MPa$\sqrt{m}$. The general crack growth direction S_G lies along the width of the page, from the right side to the left side.

in real-time by the testing machine, which were digitally recorded during the fatigue testing.

4. Results and Discussion

Figure 6(a) and (b) plot the macroscopic fatigue crack growth curves, da/dN versus ΔK, obtained for the Al-alloy tested under plane-stress and plane-strain conditions, respectively, along with the striation spacing values S_L and S_G. The so-desired 1:1 relationship between the microscopic,

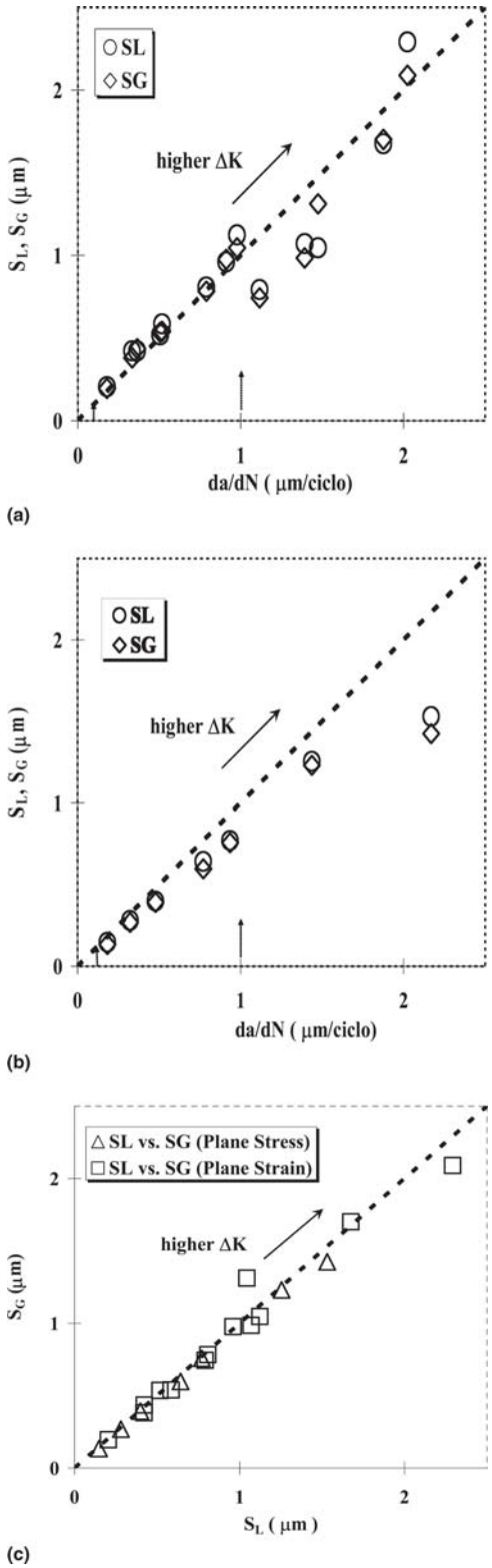

Fig. 8 Macro- and microscopic fatigue crack growth rates relationships for the material tested: (a) plane-strain; (b) plane-stress; and (c) direct comparison between measured, S_L, and general (projected), S_G, striation spacing under plane strain and plane stress conditions

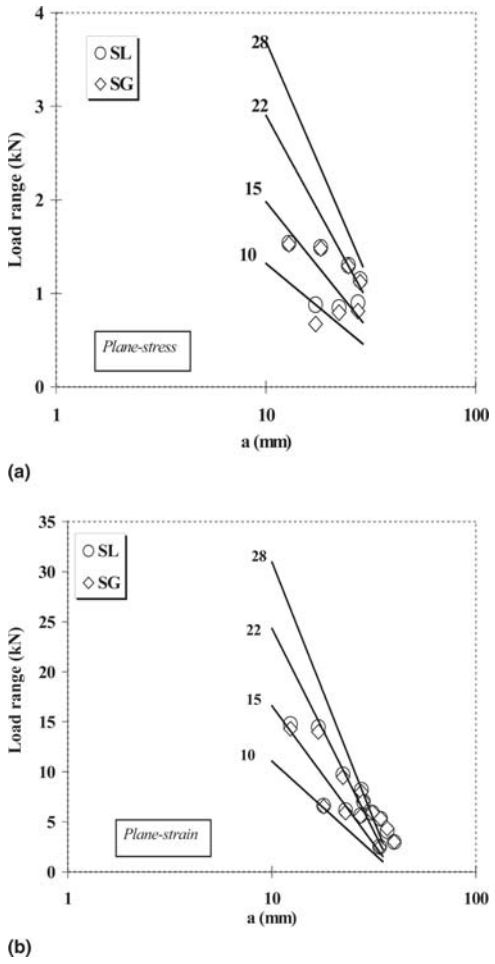

Fig. 9 K-parameterization space for (a) plane-strain 1TC(T) and (b) plane-stress 0.1T compact specimens of 7475-T7351 aluminum alloy. Four different ΔK levels have been considered in this diagram, namely 10, 15, 22, and 28 MPa.$\sqrt{m}$, denoted by the straight lines. Striation spacing in local, S_L, and general levels, S_G, are plotted as open symbols.

S, and macroscopic, da/dN, crack growth rates seems to be guaranteed. Figure 6(c) compares the macroscopic da/dN versus ΔK curves for both plane-stress and plane-strain conditions.

Figure 7 exhibits SEM-fractographs of fatigue fracture surfaces. Striation formed at three distinct and increasing ΔK levels in plane strain specimens can be observed.

Figure 8(a) and (b) plot plane-strain and plane-stress da/dN data versus S_L and S_G values, respectively. Figure 8(c) provides direct comparisons between S_L and S_G results. The diagrams confirm that microcrack and macrocrack growth rates are correlated in a 1:1 proportion up to the generally accepted limit of 1 μm/cycle (Ref 4, 5, 10). It also should be pointed out that the fair similarity between S_L and S_G values came from the fact that low ϕ angles (Eq. 1) could be afforded in this controlled-condition study. This was achieved by carefully selecting the microregions to be inspected in SEM images. This is not always the case in failure analysis investigations because adequately preserved fatigue fracture surfaces are exceptions, not the rule.

The arrows in Fig. 8(a) and (b) indicate the correlation limit in the curve da/dN × ΔK for a 1:1 relationship with striation spacing, according to Broek and Nedbal (Ref 4, 5). For prevalent plane-stress conditions, the striation spacing S_L and S_G, within the da/dN range of 0.1-1 μm/cycle (the so-called region II of fatigue crack propagation curve), are always slightly

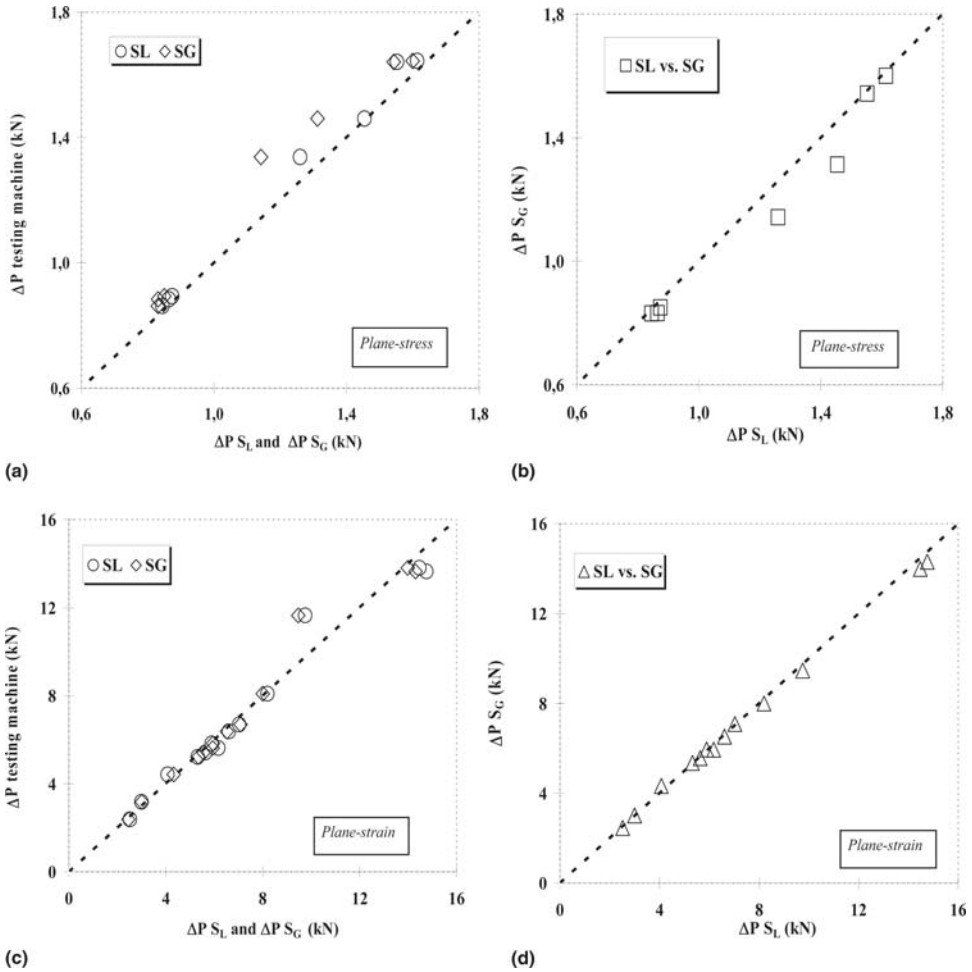

Fig. 10 Predicted load ranges, ΔP, for five ΔK levels applied during fatigue testing in plane strain conditions: (a) ΔP estimates via S_L and S_G in function of actual ΔP provided in real-time by the testing machine; (b) ΔP estimates obtained from S_L and S_G approaches, respectively; (c) and (d) the same as before, for plane-stress conditions

smaller than the macroscopic da/dN values. On the other hand, for the prevalent plane-strain conditions, an opposite trend is observed. These results suggest that the striation topography is likely to be strongly dependent on the stress-state condition; however, further studies are required to clarify the exact mechanisms governing such dependence.

As mentioned earlier, Fig. 8(c) confirms that $S_L \geq S_G$, and the relative difference between them depends on the applied ΔK value.

Figure 9 outlines the K-parameterization scheme for 0.1T and 1TC(T) specimens of Al-alloy. The diagrams refer to four distinct ΔK levels (i.e., four different da/dN values), which are represented by straight lines. Striation spacing in the local, S_L, and general, S_G, have been plotted as open symbols. It should be mentioned that the striation spacing considered in this study has been created at ΔK levels from 10-28 MPa$\sqrt{m}$.

Figure 10(a) shows predicted load ranges, ΔP, considering five distinct ΔK levels applied during fatigue testing to 1TC(T) specimens on the basis of both S_L and S_G fractographic data. In this figure, predicted ΔP ranges are plotted against the load range applied to the specimens during the fatigue crack growth tests. A very good correlation was found between predicted and actual load ranges, for both sets of data points. Figure 10(b) confirms the good similarity between ΔP-estimations determined from S_L and S_G approaches. Figure 10(c) and (d) reproduce the previously described procedure for plane-stress conditions, that is, 0.1TC(T) specimens.

Figure 11(a) plots the displacement angle ϕ between the local and general directions of striation advance, respectively S_L and S_G, against the corresponding percentage error on ΔP-estimations, relatively to the actual Δp values displayed in real-time by the fatigue testing machine. It can be observed that the vast majority of errors are lower than 10% of the load levels resulting in a subcritical crack growth process in compact specimens, which can be considered an acceptable level for estimating fatigue loads in accident failure investigations.

In the development of this work, for fatigue crack propagation in stage II, Paris' equation—$da/dN = C^*(\Delta K)^m$—and Miller correlation—$S = Cs^*(\Delta K)^{ms}$—were extensively used in all the calculations. One can observe in the line trends of Fig. 11(c) and (d), that for higher stress intensity values, the loading estimates of error are higher, for both plane stress and plane strain. This is probably due to the great influence of the maximum stress intensity factor, K_{max}, in fatigue crack propagation. In the Paris region, macroscopic fatigue crack propagation, da/dN, is influenced by K_{max} component as given by: $da/dN = C'(\Delta K_{eff})^{mr}*(K_{max})^p$ (Ref 11). As K_{max} approaches K_{IC}, the error resulting from the estimated load is increasingly larger.

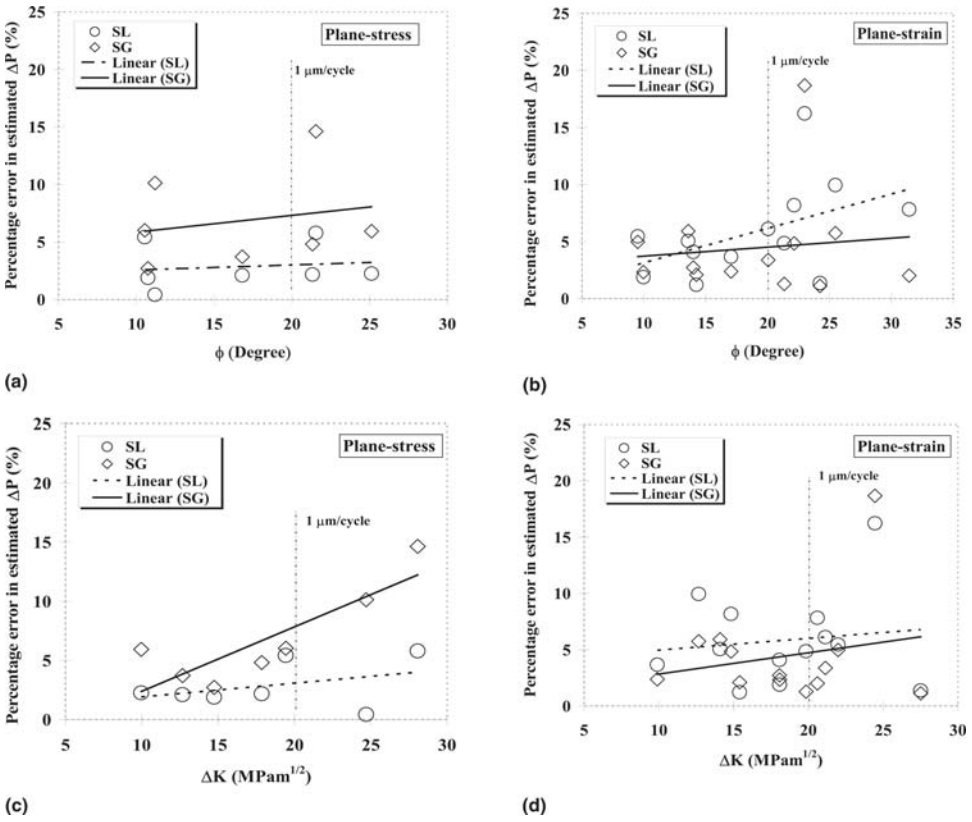

Fig. 11 Errors on estimating ΔP versus displacement angle ϕ; and versus ΔK, respectively: (a, c) plane-strain and (b, d) plane-stress conditions

5. Conclusions

This article evaluated a recently proposed procedure by which the fatigue load levels leading to failure of structural components can be estimated.

The feasibility of the Berkovitz methodology in predicting fatigue loads in laboratory-scale test specimens, under constant amplitude loading and fixed *R*-ratio, has been shown within acceptable error allowances. Therefore, the assessed procedure may be considered potentially useful in accident failure investigations, when the loading spectrum is generally not available, as long as the aforementioned loading conditions are strictly respected.

The tested model is currently being improved to account for crack closure (*R*-ratio) and variable amplitude loading (load sequence) effects. It is expected that its future adoption by the aeronautical industry can optimize all stages of aircraft manufacturing, with special emphasis to the ultimate failure analysis of in-service and full-scale testing.

Acknowledgments

The authors gratefully acknowledge CNPq and Embraer S/A for financial support. The latter is also acknowledged for providing the fatigue test specimens and promoting valuable discussions.

References

1. H. Kitagawa and R. Koterazawa, Fractography, Baifukan Inc., 1977, p 112-121
2. R. Koterazawa, The Report of the Fractography Meeting, *J. Jpn. Soc. Mech. Eng.,* 1974, **76,** p 1203-1208
3. J.B. Berkovitz, Estimation of Loads Conducting to Mechanical Failures, *Eng. Fail. Anal.,* 1995, **2,** p 215-226
4. D. Broek, *Proceedings of the 2nd International Conference on Fracture,* Chapman and Hall, 1969, p 754
5. I. Nedbal, J. Siegl, and J. Kunz, *Relation Between Striation Spacing and Fatigue Crack Growth Rate in Al-Alloy Sheets, Basic Mechanics Fatigue Metals,* IFC 7, Advances in Fracture Research, Vol. 5, Houston, TX, March 20-24, 1989, p 3483-3491
6. C.O.F.T. Ruckert, "Correlating Fatigue Striation Spacing with Load Spectrum in High-Strength SAE-AMS 7475-T7351 Aluminum Alloy," MSc. Dissertation, Engineering School of São Carlos, University of São Paulo, São Carlos, Brazil, 2003
7. "Aerospace Material Specification for Aluminum Alloy Plates, Designation SAE-AMS 4202C," 1989, p 1-9
8. "Standard Test Method for Tension Testing of Metallic Materials," E-8M, *Annual Book of ASTM Standards,* ASTM, 2000, p 77-98
9. "Standard Test Method for Measurement of Fatigue Crack Growth Rates," E-647, *Annual Book of ASTM Standards,* ASTM, 2000, p 1-37
10. C. Masuda, A. Ohta, S. Nishijima, and E. Sasaki, Fatigue Striation in a Wide Range of Crack Propagation Rates up to 70 μm/Cycle in a Ductile Structural Steel, Fatigue Testing Division, National Research Institute for Metals, p 2-3-12, Nakameguro, Meguro-Ku, Tokyo, Japan, 1980
11. R.O. Ritchie and K.T.V. Rao, Cyclic Fatigue-Crack Growth in Toughened Ceramics and Intermetallics at Ambient and Elevated Temperatures, ECF-11 Mechanisms and Mechanics of Damage and Failure, *Proceedings of the Eleventh European Conference on Fracture,* 1996, **1,** p 53-69